Institute of Paper Science and Technology
Atlanta, Georgia

IPST TECHNICAL PAPER SERIES

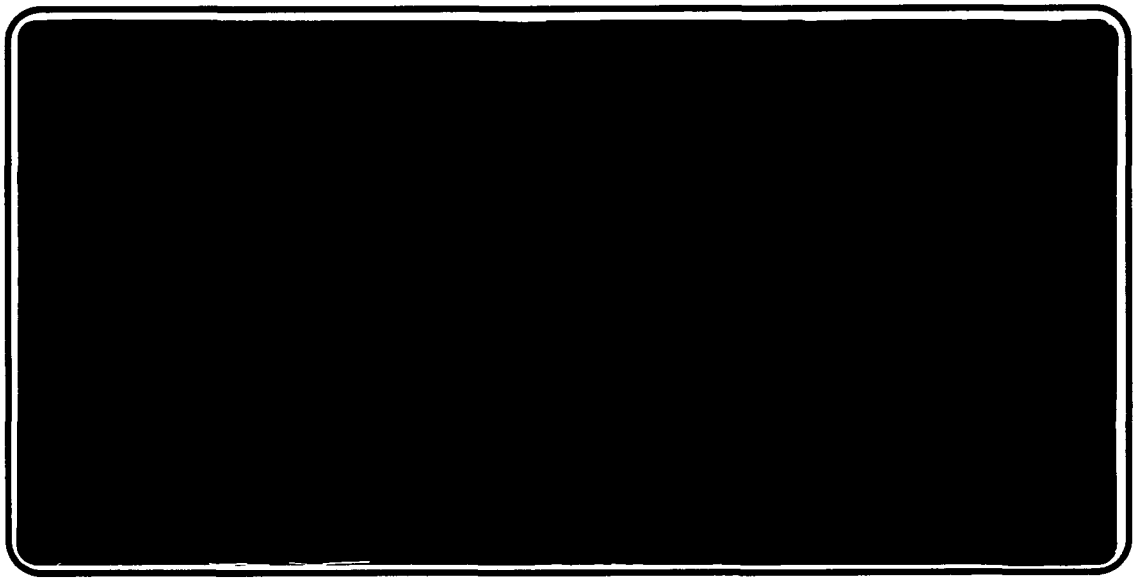

NUMBER 360

MOTION OF FLUID SUSPENDED FIBERS IN A STANDING WAVE FIELD

P. BRODEUR

SEPTEMBER, 1990

Motion of Fluid Suspended Fibers in a Standing Wave Field

P. Brodeur

Submitted for publication in

Ultrasonics

MOTION OF FLUID SUSPENDED FIBERS IN A STANDING WAVE FIELD

P. Brodeur
Paper Physics Group, Engineering and Paper Materials Division
Inst. of Paper Science and Tech.
Atlanta, GA 30318

ABSTRACT

Under the influence of a stationary ultrasonic wave field, fluid suspended fibers shorter than one-fourth of the acoustic wavelength migrate toward stable equilibrium positions and reorient to stable equilibrium angular positions. Using optical monitoring of the suspension, acoustic layering and reorientation can be studied as a function of fiber dimensions. In order to explain some experimental results obtained with a dilute water suspension of papermaking fibers, a theoretical investigation of fiber motion and light scattering behaviour during ultrasonic excitation is required. This paper reports on some aspects of the mathematical model being developed. It is shown that acoustic layering and reorientation are dominant effects for long and short fiber respectively.

Keywords: Material characterization; acoustic radiation pressure; acoustic layering and reorientation; cylindrical particles; papermaking fibers.

INTRODUCTION

When submitted to a standing wave field, fluid suspended fibers shorter than one-fourth of the acoustic wavelength migrate to preferred sites at stable equilibrium positions and reorient to stable equilibrium angular positions. The suspension takes on a striped appearance and regions of increased fiber concentration alternate with regions of decreased fiber concentration. This layering phenomenon is a consequence of acoustic radiation force. Not as clearly distinguishable, the reorientation phenomenon is due to acoustic radiation torque: fibers are reoriented in such a manner as their principal axis becomes parallel to the layer planes. Although acoustic layering and reorientation are not dissociable processes, they have different characteristic times.

While much attention has been given in the past to acoustic radiation pressure effects in general[1,2] and on spheres and discs,[3,4,5] lack of practical interest in cylinders irradiated by ultrasonic waves has limited the literature on this particular subject. In fact, only recently has acoustic rearrangement of cylinders received an experimental impetus with the development of an acousto-optical method to measure some properties of water suspended papermaking fibers (exceeding 3 mm in length); more precisely, correlations were established between average fiber dimensions and scattered light measurements recorded during acoustic

excitation[6,7,8,9]. Analytical expressions describing acoustic radiation force on a rigid cylinder in a plane progressive wave were derived by Awatani[10], Zhuk[11] and Hasegawa et al.[12] The motion of a rigid cylinder due to a plane elastic wave was studied by Miles[13]. An expression describing the acoustic radiation force on a cylinder whose principal axis is perpendicular to the direction of a plane standing wave was recently developed by Wu et al.[14] While no formal theory is yet available to explain cylinder reorientation due to acoustic radiation torque, Putterman et al.[15] have derived a best fit equation to predict the torque on a levitated cylinder positioned in a loop. Regarding particle motion in a standing wave field, ter Harr and Wyard[16] have proposed a model for banding of spherical blood cells. Svirkunov[17] has carried out a physical analysis of particle motion in a standing wave field formed by counterpropagating waves with slightly different frequencies.

This paper presents a mathematical model to explain some experimental results obtained with papermaking fibers in a standing wave field[8]. The analysis is considerably simplified by assuming a dilute suspension of rigid circular cylinders. First, translational and angular motions of fibers due to acoustic radiation pressure effects are studied separately. Then, in agreement with optical monitoring of the suspension, layering and reorientation contributions to the scattered light are derived. These contributions are combined to predict the composite scattered light observed during ultrasonic excitation.

MATHEMATICAL MODEL

Linear and Angular Velocities Due to Acoustic Radiation Pressure

Consider a fluid-filled resonator in which a plane standing wave field with acoustic wavelength λ propagates horizontally. Neglecting the presence of gas bubbles, temperature effects, wave distortion (Oseen-type forces) and buoyancy forces, a fluid suspended rigid circular cylinder with radius a and length $\ell >> a$ and $<< \lambda$ reacts to forces and torques due to acoustic radiation pressure and viscous drag. In the general situation in which the cylinder has an initial random orientation, the acoustic radiation force analysis can be quite complicated. Fortunately, if one makes the assumption (verified experimentally) that acoustic reorientation is a faster process than acoustic displacement, the cylinder quickly rotates so that its principal axis becomes perpendicular to the wavefront propagation axis for most of its migration. Under this condition, the analytical result developed by Wu et al.[14] for the case of a unit length circular cylinder in a frictionless medium can be used. Their quoted expression for the acoustic radiation force F_{sw} is

$$F_{sw} = f(\beta) \frac{\pi a^2}{2} \overline{E} \, k \sin[2kh] \qquad (1)$$

where $f(\beta) = [\,[2(1-\beta)/(1+\beta)] + 1]$ is the inertia factor, $\beta = \rho_0/\rho_1$ is the ratio of the equilibrium density of the suspending medium to the cylinder density, $\overline{E}$ is the mean acoustic energy-density, $k = 2\pi/\lambda$ and h is the cylinder center of mass position with respect to a reference plane. For the case of papermaking fibers in a water suspension, $\beta \approx 1$ and, therefore, $f(\beta)$ and F_{sw} are positive. As illustrated in Figure 1, in which nodes (N) at zero particle velocity are located at $x = h_N = n\lambda/2$, $n = 0, \pm1, \pm2$ ... and loops (L) are situated at $x = h_L = (n + 1/2)\,\lambda/2$, $n = 0, \pm1, \pm2$ ..., F_{sw} is maximum halfway between nodes and loops and it is directed toward loops. In other words, papermaking fibers should migrate toward the nearest loops at stable equilibrium positions; this is confirmed by experimental observation. F_{sw} is positive in the remainder of this paper.

Assuming now a Newtonian fluid at rest with viscosity μ, the cylinder experiences a retarding force F_d. Neglecting any radius dependency, the drag force for a unit length cylinder whose axis is perpendicular to the wavefront in the laminar regime (Reynold's number $N_R = \rho_0(2a)v/\mu$ less than one) is[18,19]

$$F_d = 2\,\pi\,C\,\mu\,v(h) \tag{2}$$

where C is a numerical constant and $v(h) = dh/dt$ is the cylinder migration velocity. The equation of motion has the form,

$$m_1 \frac{d^2h}{dt^2} = F_{sw} - F_d \tag{3}$$

where m_1 is the mass of the cylinder. If the accelerating force can be neglected, then equations (1) and (2) can be equated, and v(h) is expressed as

$$v(h) = A\,\overline{E}\,k\,a^2 \sin[2kh] \tag{4}$$

in which A is a constant. Equation (4) shows that at constant mean acoustic energy-density and wave vector, the larger the square of the cylinder radius is, the larger the velocity is at a given position h.

The acoustic radiation torque acting on a cylinder in a standing wave field originates from the acoustic force gradient denoted between nodes and loops. As seen in Figure 1, the axis of rotation is the Y-axis and θ is defined as the angle between the direction of propagation of the wavefront (X-axis) and the normal to the cylinder principal axis. According to King[5] and Putterman et al.[15] the torque acting on a non-spherical object in a standing wave field is proportional to its volume and the mean acoustic energy-density. King[5] has shown that the couple on a thin circular disc for which $ka << 1$ (a is the disc radius) situated in a node is of a much smaller order of magnitude than that exerted on it in a loop, and is of opposite sign. One should

expect something similar for a rotating cylinder. As a first approximation, the small magnitude torque in the node vicinity can be neglected. Hence, for a cylinder located at position h, we have

$$T_{sw} \propto - V \bar{E} \sin[2\theta] \sin^2[kh] \tag{5}$$

where $V = \pi a^2 \ell$ is the cylinder volume. The torque is negative with respect to θ and its magnitude increased as a function of h. The stable equilibrium angular position is at $\theta = 0$. When positioned at $h = h_L$, the cylinder is at a stable equilibrium spatial position and cannot rotate. Using equation (2) one finds an expression for the drag torque acting on a cylinder of length ℓ,

$$T_d \propto \mu \ell^3 \omega(\theta) \tag{6}$$

Neglecting cylinder inertia, we have an expression for the cylinder reorientation velocity,

$$\omega(\theta) = - B \bar{E} \left(\frac{a}{\ell}\right)^2 \sin\left[2\theta\right] \sin^2[kh] \tag{7}$$

in which B is a constant. This equation indicates that the larger the square of the radius or the shorter the square of the length, the faster the cylinder reorients to a stable equilibrium angular position.

Spatial and Angular Distributions of Cylinders

Based on the above initial considerations for one cylinder, the model can be extended to a cylinder suspension in which the center of mass and initial orientation of cylinders are randomly distributed. More specifically, the behaviour of a dilute suspension is analysed. Defining c as the fraction of the total volume of the suspension occupied by the cylinders, a suspension is dilute when $c < (2a/\ell)^2$, i.e. when the distance between a cylinder and its nearest neighbor is greater than ℓ[20]. In that regime, interactions between cylinders are rare and they are free to rotate.

The spatial distribution function f(h,t) along the X-axis ($h_N \leq h \leq h_L$) is derived from the equation of continuity,

$$\frac{\partial f(h,t)}{\partial t} = - \frac{\partial [f(h,t)\, v(h)]}{\partial h} \tag{8}$$

One gets upon substitution of (4) into (8) and after integration,

$$f(h,t) = \frac{f_0}{\sin^2[kh]\exp[-2A\bar{E}(ka)^2t] + \cos^2[kh]\exp[2A\bar{E}(ka)^2t]} \qquad (9)$$

Here f_0 is the initial distribution of cylinders at t = 0. Figure 2 represents a three-dimensional plot of f(h,t) for arbitrary constant mean acoustic energy-density, wave vector and cylinder radius. As time increases, the distribution goes rapidly to infinity at $h = h_L$. This unrealistic effect is a consequence of a continuous distribution and it is easily suppressed by assuming a discrete distribution of finite dimension cylinders. Nevertheless, Figure 2 is a good indication of the migration process. Integrating f(h,t) with respect to h over the spatial window $(h_L - s) \leq h \leq h_L$ where $0 \leq s \leq \lambda/4$ (see Figure 4) provides some insight about the integrated distribution of cylinders as a function of time in the vicinity of stable equilibrium positions. We carry out the integration to obtain after some manipulations,

$$F(t) = \frac{f_0}{k}\tan^{-1}[\tan[ks]\exp[2A\bar{E}(ka)^2t]] \qquad (10)$$

If $s = \lambda/4$, then $F(t) = f_0 s$, i.e., time independent as we expect. Since every cylinder has a discrete position h_0 at t = 0, its trajectory as a function of time is easily obtained from equation 10. Replacing s by the final position $\lambda/4 - h'$ at time t, F(0) by $\lambda/4 - h_0$ and f_0 by 1 (only one particle), we have,

$$h' = \frac{1}{k}\tan^{-1}[\tan[kh_0]\exp[2A\bar{E}(ka)^2t]] \qquad (11)$$

This equation implies that cylinder superposition is allowed at $h_0 = h_L$. The difficulty is easily solved by imposing a particle dimension constraint on the trajectories. Figure 3 depicts selected trajectories for equally distant cylinders at t = 0.

Analysis of the angular distribution of randomly oriented cylinders in the X-Z plane (see Figure 1) is performed in a similar manner as for the spatial distribution. In that case, the governing equation depends on the conservation of fiber orientation[21]. For the angular range $0 \leq \theta \leq \pi/2$, the distribution function $g(\theta,t)$ is

$$g(\theta,t) = \frac{g_0}{\sin^2[\theta]\exp[2B\bar{E}(a/\ell)^2\sin^2[kh]\,t] + \cos^2[\theta]\exp[-2B\bar{E}(a/\ell)^2\sin^2[kh]\,t]} \qquad (12)$$

where g_0 is the initial angular distribution. The integrated angular distribution of cylinders as a function of time for the arbitrary range $0 \leq \theta \leq \varphi$, $\varphi \leq \pi/2$ is

$$G(t) = g_0 \tan^{-1}\left[\tan[\varphi] \exp\left[2B\bar{E}(a/\ell)^2 \sin^2[kh]t\right]\right] \quad (13)$$

As for trajectories, an equation is available to describe the reorientation of a cylinder with an initial angular position θ_0 at t = 0. If φ is replaced by θ' at time t, G(0) by θ_0 and g_0 by 1, the angular position of a cylinder at any time t during acoustic rearrangement is

$$\theta' = \tan^{-1}\left[\tan[\theta_0] \exp\left[-2B\bar{E}(a/\ell)^2 \sin^2[kh]t\right]\right] \quad (14)$$

Equations (11) and (14) define the translational and angular motions of a single cylinder in a stationary ultrasonic wave field. Since they have different characteristic times, a graphical representation of the composite motion is of little interest. In fact, acoustic rearrangement is best monitored by small-angle forward light scattering[8], and one should look for relationships between the integrated spatial and angular distributions (equations 11 and 13) and their respective light scattering contributions. Before addressing this issue, it is necessary to briefly review the experimental setup developed to study acoustic radiation pressure effects on papermaking fibers suspended in water.

Experimental Setup

The experimental work reported in this paper was performed at Universite du Quebec a Trois-Rivieres (Canada). It has been described in detail elsewhere[8,9]. A partial view of the experimental setup is presented in Figure 4. A collimated beam of incandescent light propagating in the Z-direction illuminates the fiber suspension. Fibers are suspended in degassed water. The acoutic resonator (not shown in the figure) is along the X-direction, i.e., perpendicular to the collimated beam axis on the horizontal plane. It is operated in a continuous mode during a period of 20 s at constant mean acoustic energy-density; the acoustic power is not monitored. As the acoustic wavelength is set to 20 mm (the resonant frequency is 72 kHz), fibers up to 5 mm in length ($\lambda/4$) can be analysed. Vertical narrow slits with halfwidth s located at the entrance window of the measuring cell (see Figure 4) are used to produce thin layers of light coincident with expected fiber layer positions (loop planes). Small-angle scattered light from fibers located at loop planes is collected on the X-axis. In this manner, assuming a linear relationship between fiber consistency and light scattering during ultrasonic excitation, scattered light measurements provide a direct way to monitor the layering process. However, because this detection scheme fails to fully discriminate between the layering and reorientation effects, composite light signals are actually observed. No attempt was made to get independent fiber orientation measurements.

Light Scattering Modeling

The composite scattered light intensity from the layering and reorientation effects at any time during ultrasonic excitation can be defined as

$$I(t) = I_F(t) + I_G(t) \tag{15}$$

where $I(0) = I_0$ is the initial scattered light intensity, $I_F(0) = pI_0$ is the layering contribution, $I_G(0) = (1-p)I_0$ is the reorientation component and p is a weighting factor ranging between 0 and 1. If the initial spatial distribution f_0 in equation (10) is linearly related to I_0, $I_F(t)$ is given by,

$$I_F(t) = \frac{pI_0}{ks} \tan^{-1}\left[\tan[ks] \exp\left[2A\bar{E}(ka)^2 t\right]\right] \tag{16}$$

where normalization to the width s of the spatial window has been applied. A similar equation is available for $I_G(t)$. Normalizing equation (13) to the arbitrary angular range φ, we obtain,

$$I_G(t) = \frac{(1-p)I_0}{\varphi} \tan^{-1}\left[\tan[\varphi] \exp\left[2B\bar{E}(a/\ell)^2 \sin^2[kh]t\right]\right] \tag{17}$$

EXPERIMENTAL RESULTS

Any attempt to describe papermaking fibers by rigid circular cylinders is a rather crude approximation because wood fibers have a tapered cross-section and may be curled and fibrillated. Their dimensions are generally described by average length and cross-section. It appears from data collected from several wood species that coarseness of wood fiber is, on the average, reasonably proportional to its length[22]. Since coarseness is a measure of cross-section and, therefore, is related to the square of an effective radius, fiber length is approximately proportional to the square of radius for papermaking fibers. This empirical relationship has undesirable consequences in the present work because it complicates the observation of distinctive effects of length and radius as predicted by the model.

Stone groundwood mechanical pulp fibers were used in all experiments. Measurements were performed on the whole pulp (original stock) and six standard length classified pulp fractions obtained from a differential screen classifier (Bauer-McNett classifier). Fraction percentages and respective standard lengths[23] are tabulated in Table 1. The whole pulp average length is calculated by summing fraction lengths multiplied by fraction percentages. Although the P200 fraction refers to fines or debris in the pulp (rejects from the screen classifier), an average

length of 0.2 mm is attributed to this fraction[23]. In order to collect measurements in agreement with a dilute suspension regime, fiber consistency is set to 0.0005% for all fractions. At this low level, consistency is linearly related to scattered light before and during acoustic rearrangement[8].

Average scattered light intensity measurements as a function of time for the whole pulp and fractions are presented in Figure 5. Curves are normalized to identical initial intensity level. One can see that the larger the average fiber length, the faster the fibers move toward stable equilibrium positions. While the layering process is almost completed within the 20 s time interval for the longest fibers, it is far from being completed for the fines (order of several minutes). An interesting observation is the ordering inversion of the P200 and L200 curves during the first 9 seconds. As explained below with the model, this is due to a dominant reorientation effect for the fines. As time goes on, scattered light attributed to this effect is rapidly saturating while the layering contribution keeps increasing at a much slower rate.

NUMERICAL RESULTS AND DISCUSSION

Scattered light measurements gathered without ultrasonic excitation for all pulp fractions show that I_0 is inversely proportional to the fraction average length[8]. This is also verified for the whole pulp. Since the entrance slits in the experimental setup have a 0.5 mm halfwidth ($0.1\lambda/4$), the spatial window s in equation (16) is a known quantity. Assuming that scattered light intensity is essentially due to fibers oriented in a direction parallel to the light propagation axis (parallel to layer planes), one can define an arbitrary effective angular range $0 \le \varphi \le \varphi'$ in equation (17). A reasonable estimate for φ' is $0.1\pi/2$, i.e., 10% of the maximum angular range. Upon substitution of equations (16) and (17) in (15), the predicted composite scattered light intensity I(t) for wood fibers of length l is

$$I(t) = I(\ell,t) \propto \frac{20p}{\pi\ell} \tan^{-1}\left[\tan[\pi/20] \exp[A'\ell\, t]\right] + \frac{20(1-p)}{\pi\ell} \tan^{-1}\left[\tan[\pi/20] \exp[B't / \ell]\right] \qquad (18)$$

where a^2 has been replaced by ℓ as discussed earlier. This equation has three unknown parameters: p, A' and B'. Approximate values for these parameters are found by adjusting experimental curves (Figure 5) and calculated curves normalized to identical intensity levels for all fractions using equation (18). The predicted unnormalized scattered light intensity variations versus time are presented due to layering (Figure 6), reorientation (Figure 7), and combined layering and reorientation (Figure 8). The predicted normalized variations due to combined layering and reorientation are presented in Figure 9. The following parameter values were used in the calculations: $p = 0.96$, $A' = 0.08$ and $B' = 0.07$. In each

figure, the whole pulp curve is computed by summing fraction curves multiplied by their percentage. Considering the many assumptions involved in the present work, it is quite satisfactory to predict the general trend of the experimental data. While values for A' and B' are arbitrary, a value close to one for the weighting factor p indicates that scattered light attributed to reorientation is a small correction factor to the layering contribution. This is true of all fractions to the exception of fines (P200 fraction), in which case reorientation is initially dominant. The model is capable of predicting the L200 and P200 curves ordering inversion. This is an indication that, for papermaking fibers, the migration velocity v(h) (equation 4) is proportional to ℓ and the reorientation velocity $\omega(\theta)$ (equation 7) is inversely proportional to ℓ. The largest discrepancy between experimental and predicted curves is denoted for the longest fibers (L14 fraction); this is most likely a consequence of the less precise recordings for that fraction because the number of L14 fibers is quite small at 0.0005% consistency.

CONCLUSION

A model taking into account acoustic layering and reorientation processes was developed to explain experimental results obtained with water suspended papermaking fibers subjected to ultrasonic standing waves. The model shows that layering and reorientation are dominant effects for long and short fibers, respectively. Since fiber length and radius are related for wood fibers, it was not possible to fully test the model against these two quantities. In the future, a more complete investigation of the model might include measurements with variable mean acoustic energy-density, variable acoustic wavelength and adjustable entrance slit width and position. Also, measurements with cylinder-like fibers of variable length and constant radius and constant length and variable radius are required. Finally, it is believed that a full understanding of acoustic radiation pressure effects acting on fibers in a dilute suspension regime could be the basis for the physical analysis of fiber acoustic rearrangement in a semi-concentrated regime.

ACKNOWLEDGMENTS

The author wishes to thank Professors J.F. Waterhouse and M.S. Hall of the Institute of Paper Science and Technology for their helpful discussions.

BIBLIOGRAPHY

1. Westervelt, P.J.. Acoustic Radiation Pressure. J. Acoust. Soc. Am. 29:26-29(1957).

2. Maidanik, G. Torques Due to Acoustic Radiation Pressure. J. Acoust. Soc. Am. 30:620-623(1958).

3. King, L.V. On the Acoustic Radiation Pressure on Spheres. Proc. R. Soc. London. 147A:212-240(1934).

4. King, L.V. On the Acoustic Radiation Pressure on Circular Discs: Inertia and Diffraction Corrections Proc. R. Soc. London. 153A:1-16(1935).

5. King, L.V. On the theory of the inertia and diffractions corrections for the Rayleigh disc Proc. R. Soc. London 153A 17-40(1935).

6. Dion, J.L., Valade, J.L. and Law, K.N. Evolution d'une suspension de fibres dans un champ ultrasonore stationnaire Acustica 65 284-289(1988).

7. Dion, J.L., Brodeur, P., Garceau, J.J. and Chen, R. Caracterisation acousto-optique des fibres: nouveaux resultats J. Pulp Paper Sc. 14 J143-J144(1988).

8. Brodeur, P., Dion, J.L., Garceau, J.J., Pelletier, G. and Massicotte, D. Fibre characterization in a stationary ultrasonic field IEEE Trans. Ultrason. Ferroelec. Freq. Control 36 549-553(1989).

9. Garceau, J.J., Dion, J.L., Brodeur, P. and Luo, H. Acousto-optical fiber characterization Tappi J. 72 171-173(1989).

10. Awatani, J. Study on acoustic radiation pressure (VI), radiation pressure on a cylinder J. Acous. Soc. Japan 9 140-146(1953).

11. Zhuk, A.P. Radiation force acting on a cylindrical particle in a sound field Sov. Appl. Mech. 22 689-693(1987).

12. Hasegawa, T., Saka, K., Inoue, N. and Matsuzawa, K. Acoustic radiation force experienced by a solid cylinder in a plane progressive sound field, J. Acoust. Soc. Am. 83 1770-1775(1988).

13. Miles, J.W. Motion of a rigid cylinder due to a plane elastic wave, J. Acoust. Soc. Am. 32 1656-1659(1960).

14. Wu, J., Du, G., Work, S.S. and Warshaw, D.M. Acoustic radiation pressure on

a rigid cylinder: An analytical theory and experiments, J. Acoust. Soc. Am. 87 581-586(1990).

15. Putterman, S., Rudnick, J. and Barmatz, M. Acoustic levitation and the Boltzmann-Ehrenfest principle J. Acoust. Soc. Am. 85 68-71(1989).

16. ter Harr, G. and Wyard, S.J. Blood cell banding in ultrasonic standing wave fields: a physical analysis Ultrasound in Med. & Biol. 4 111-123(1978).

17. Svirkunov, P.N. Motion of small particles at the nodes of acoustic waves Sov. Phys. Tech. Phys. 32 678-679(1987).

18. Batchelor, G.K. An Introduction to Fluid Dynamics Camb. U. Press, Cambridge 615p.(1967).

19. Finn, R.K. Determination of the drag on a cylinder at low Reynold's numbers J. Appl. Phys. 24 771-773(1953).

20. Folgar, F. and Tucker III, C.L. Orientation behaviour of fibers in concentrated suspensions J. Reinf. Plast. Compos. 3 98-119(1984).

21. Altan, M.C., Advani, S.G., Guceri, S.I. and Pipes, R.B. On the description of the orientation state for fiber suspensions in homogeneous flows J. Rheol. 33 1129-1155(1989).

22. d'A. Clark, J. Some thoughts on fiber classification and length Tappi J. 68 119-121 (1985).

23. Tasman, J.E. The fiber length of Bauer-McNett screen fraction Tappi J. 55 136-138(1972).

FIGURE CAPTIONS

Figure 1. Acoustic radiation force and torque acting on a cylinder in a stationary ultrasonic wave field. N and L refer to nodal and loop planes, respectively.

Figure 2. 3D plot of the one-dimensional distribution function f(h,t). The position zero is at a nodal plane.

Figure 3. Selected trajectories as a function of time for equally distant cylinders at t = 0. The simulation assumes finite dimensions particles.

Figure 4. Schematic of the experimental setup used to analyse water suspended papermaking fibers. The acoustic wavefront propagation direction is along the X-axis.

Figure 5. Normalized scattered light intensity variations recorded during ultrasonic excitation for the various pulp fractions and the whole pulp. The initial time corresponds to the end of a 60 s waiting period to allow turbulence slowing down in the suspension. This Figure was reproduced from ref. 8.

Figure 6. Predicted unnormalized scattered light intensity variations for the layering contribution.

Figure 7. Predicted unnormalized scattered light intensity variations for the reorientation contribution.

Figure 8. Predicted unnormalized composite scattered light intensity variations.

Figure 9. Curves of Figure 8 normalized to identical initial intensity levels. These curves are to be compared with the experimental results shown in Figure 5.

Table 1. Data relative to stone groundwood pulp fibers for the six fractions available and the whole pulp (W.P.). Length figures are standard values for Bauer-McNett screen classifier. Coarseness was not measured.

Fraction	L14	L28	L48	L100	L200	P200	W. P.
%	1.5	10.5	20.2	17.9	14.7	35.2	100
Length (mm)	3.05	2.00	1.23	0.70	0.35	0.2	0.75

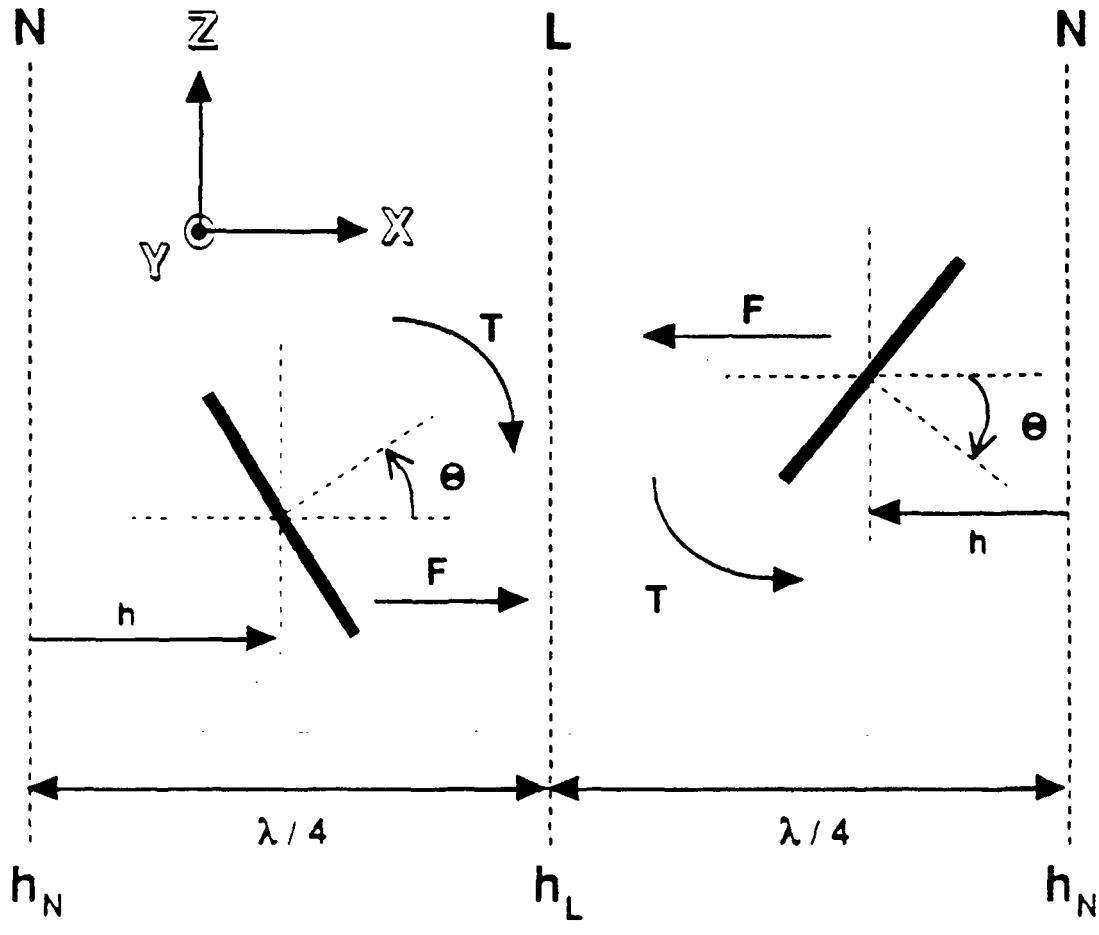

Figure 1. Acoustic radiation force and torque acting on a cylinder in a stationary ultrasonic wave field. N and L refer to nodal and loop planes, respectively.

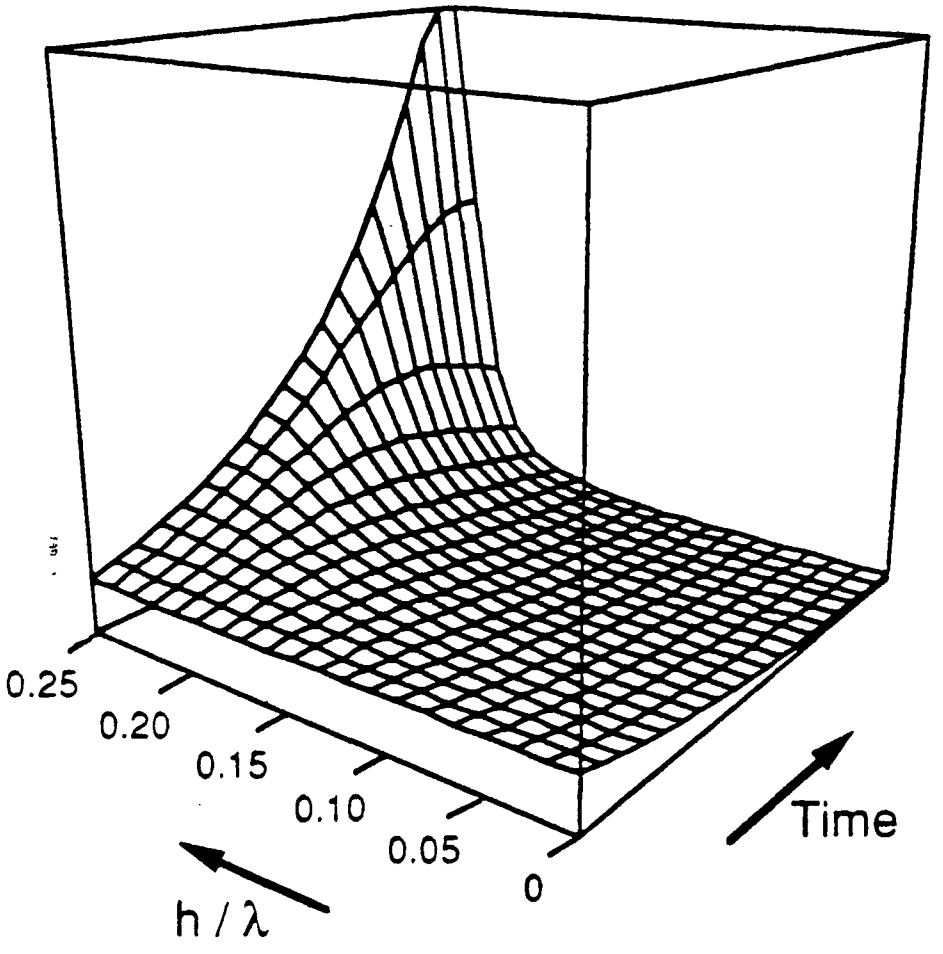

Figure 2. 3D plot of the one-dimensional distribution function f(h,t). The position zero is at a nodal plane.

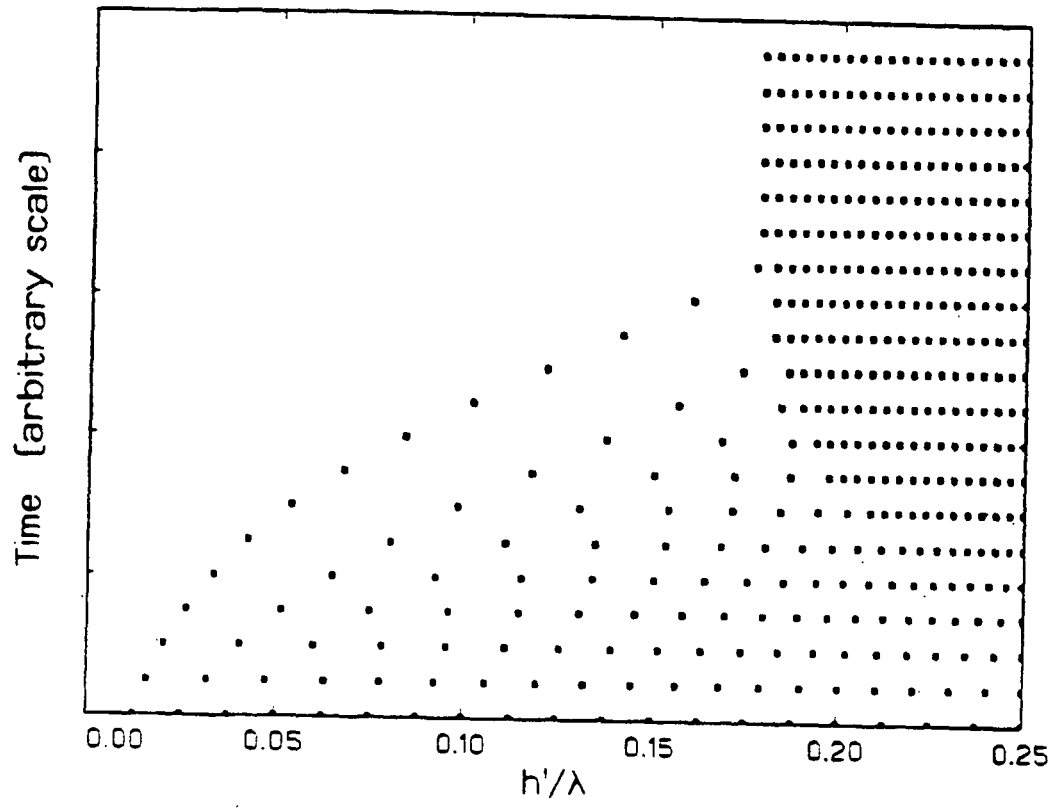

Figure 3. Selected trajectories as a function of time for equally distant cylinders at t = 0. The simulation assumes finite dimensions particles.

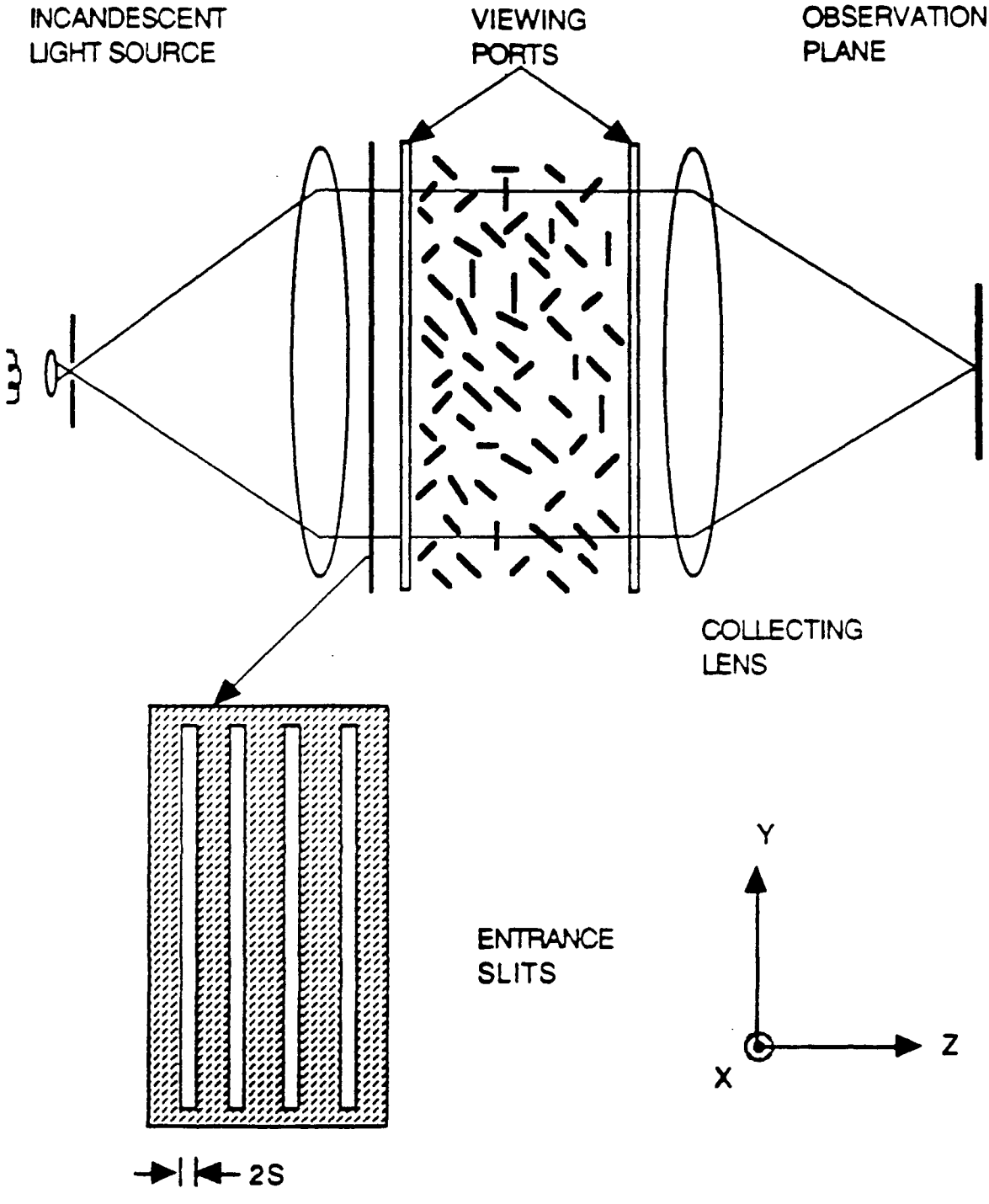

Figure 4. Schematic of the experimental setup used to analyse water suspended papermaking fibers. The acoustic wavefront propagation direction is along the X-axis.

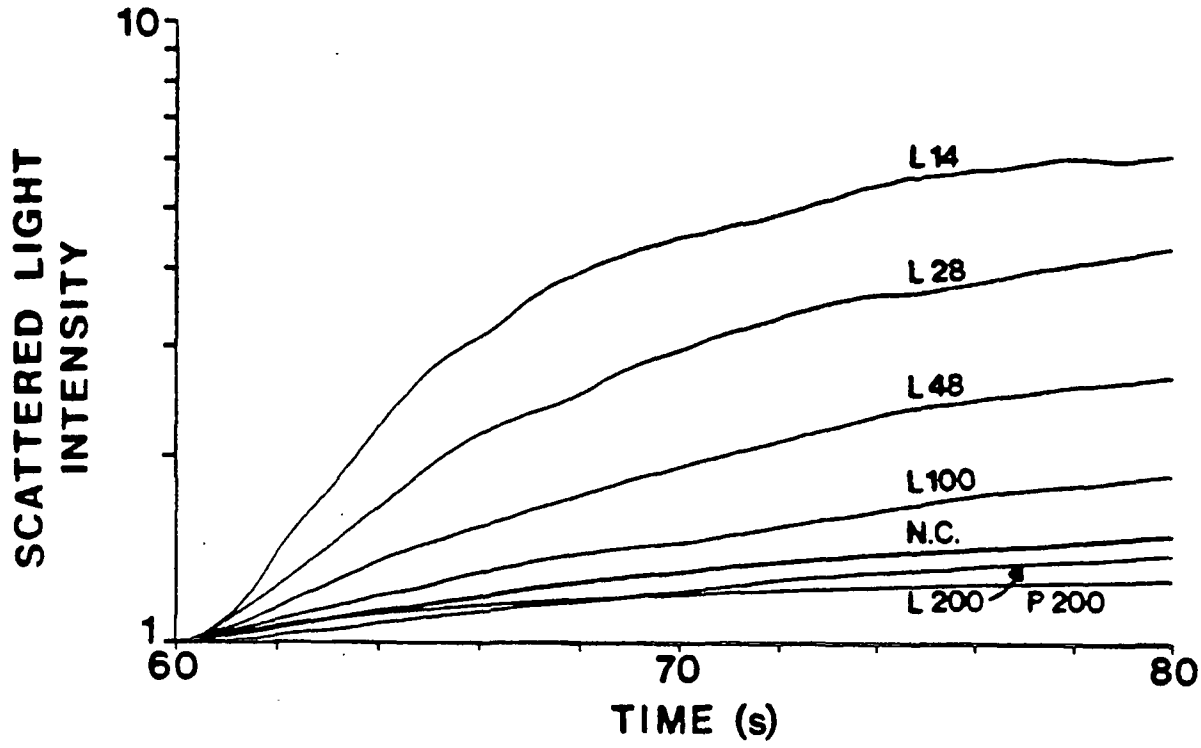

Figure 5. Normalized scattered light intensity variations recorded during ultrasonic excitation for the various pulp fractions and the whole pulp. The initial time corresponds to the end of a 60 s waiting period to allow turbulence slowing down in the suspension. This Figure was reproduced from ref. 8.

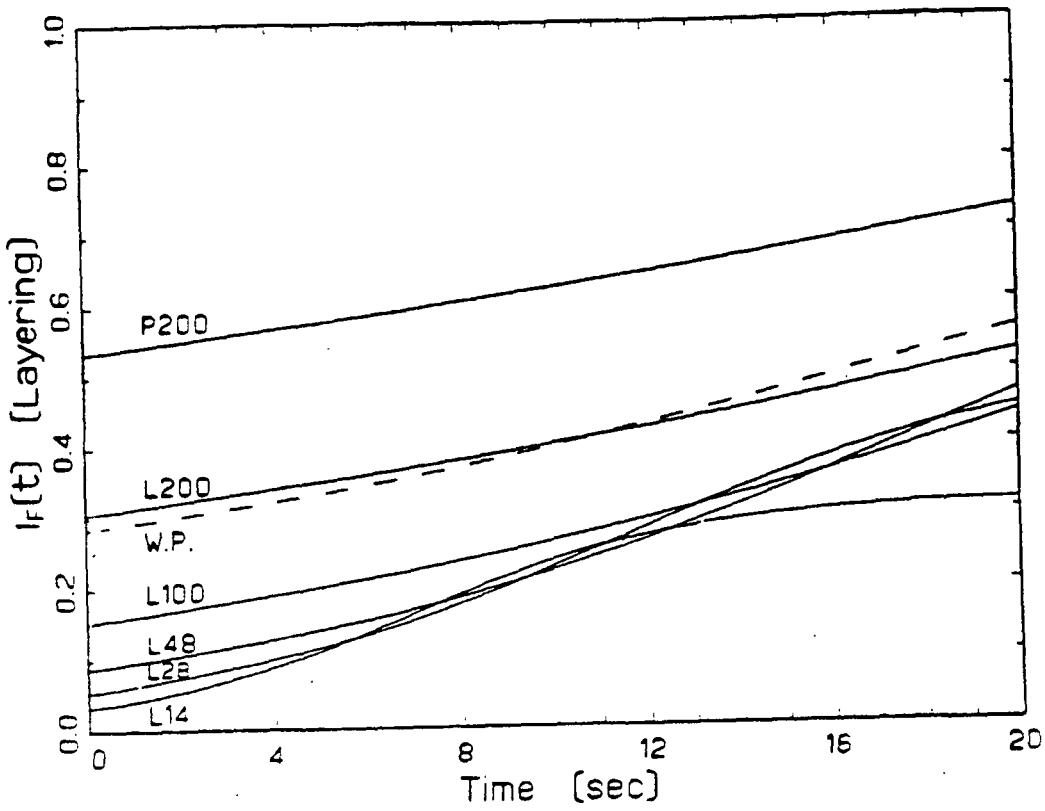

Figure 6. Predicted unnormalized scattered light intensity variations for the layering contribution.

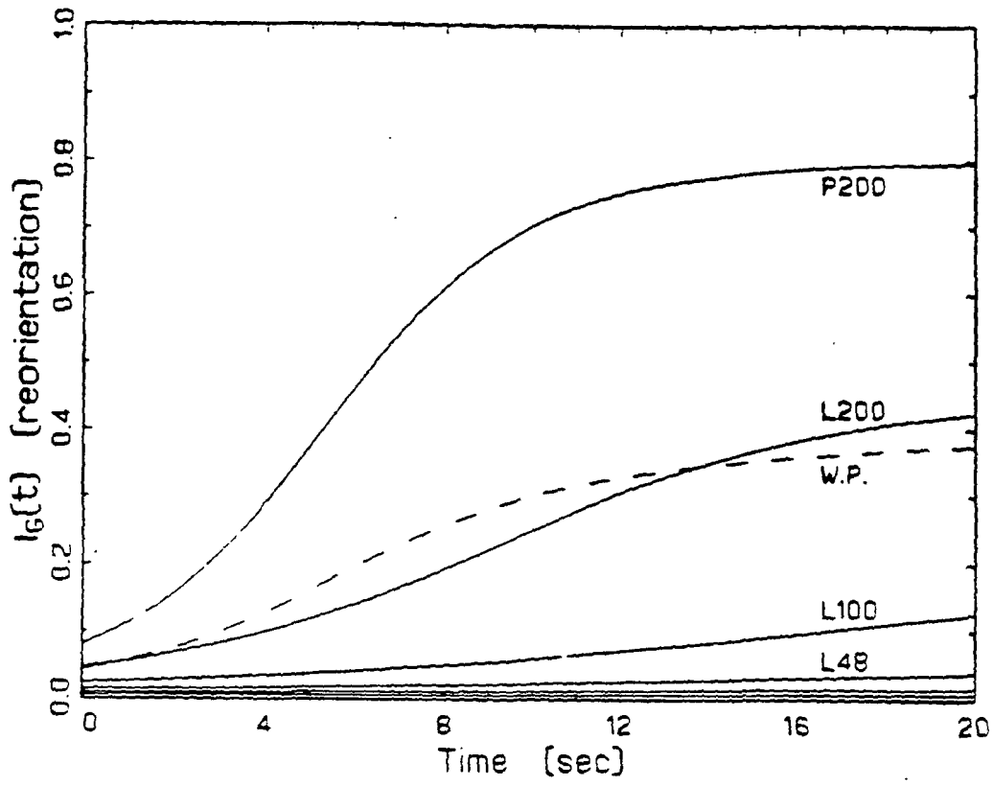

Figure 7. Predicted unnormalized scattered light intensity variations for the reorientation contribution.

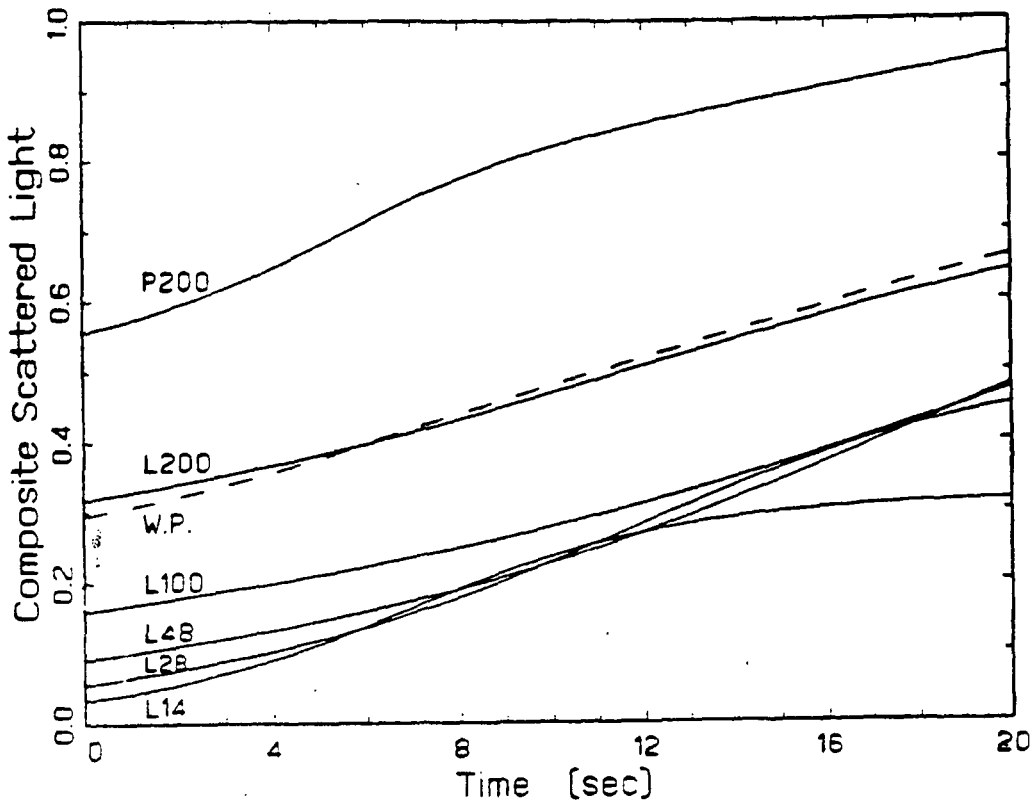

Figure 8. Predicted unnormalized composite scattered light intensity variations.

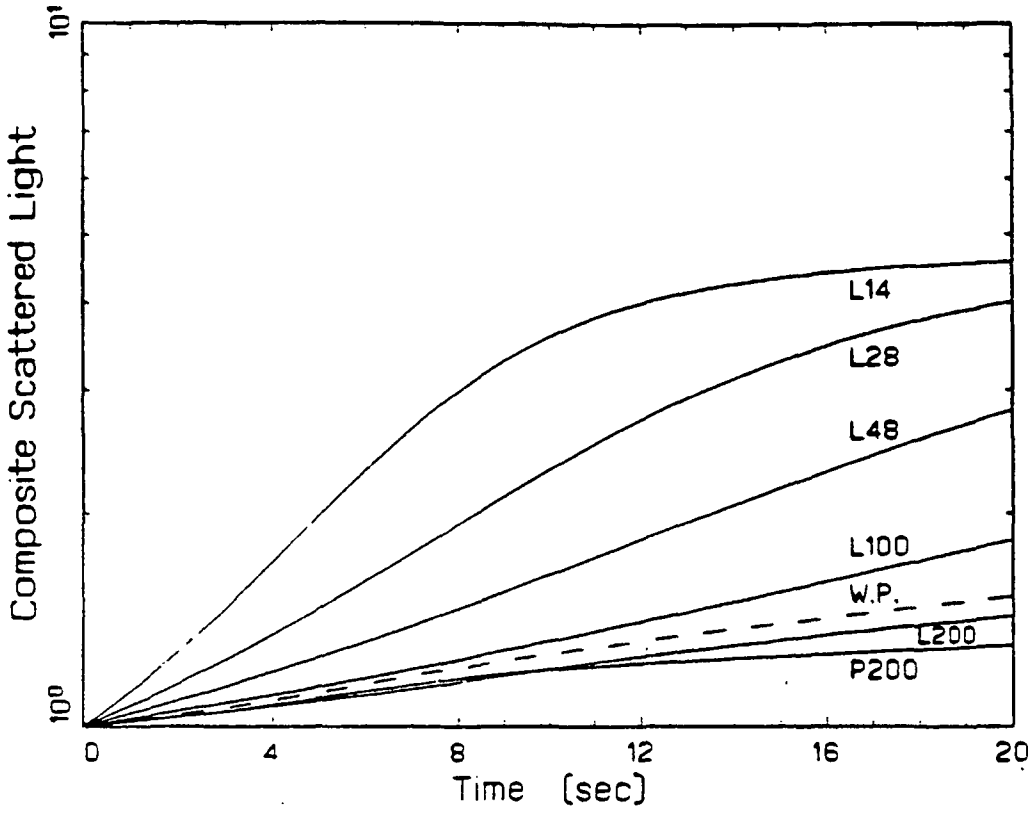

Figure 9. Curves of Figure 8 normalized to identical initial intensity levels. These curves are to be compared with the experimental results shown in Figure 5.